HHS Public Access

Author manuscript

Neuron. Author manuscript; available in PMC 2016 September 23.

Published in final edited form as:

Neuron. 2015 September 23; 87(6): 1261–1273. doi:10.1016/j.neuron.2015.08.030.

Stochastic interaction between neural activity and molecular cues in the formation of topographic maps

Melinda T. Owens[1], **David A. Feldheim**[2], **Michael P. Stryker**[1], and **Jason W. Triplett**[2,3,*]

[1]Center for Integrative Neuroscience and Departments of Physiology and Bioengineering & Therapeutic Sciences, University of California, San Francisco, San Francisco, CA 94143

[2]Molecular, Cell & Developmental Biology, University of California, Santa Cruz, Santa Cruz, CA 95064

[3]Center for Neuroscience Research, Children's National Health System, Washington, DC 20010

SUMMARY

Topographic maps in visual processing areas maintain the spatial order of the visual world. Molecular cues and neuronal activity both play critical roles in map formation, but their interaction remains unclear. Here, we demonstrate that when molecular- and activity-dependent cues are rendered nearly equal in force, they drive topographic mapping stochastically. The functional and anatomical representation of azimuth in the superior colliculus of heterozygous *Islet2-EphA3* knock-in ($Isl2^{EphA3/+}$) mice is variable: maps may be single, duplicated, or a combination of the two. This heterogeneity is not due to genetic differences, since map organizations in individual mutant animals often differ between colliculi. Disruption of spontaneous waves of retinal activity resulted in uniform map organization in $Isl2^{EphA3/+}$ mice, demonstrating that correlated spontaneous activity is required for map heterogeneity. Computational modeling replicates this heterogeneity, revealing that molecular- and activity-dependent forces interact simultaneously and stochastically during topographic map formation.

INTRODUCTION

In the visual system, the spatial relationships of objects in the world are faithfully relayed throughout higher processing centers through the establishment of topographic maps (Cang and Feldheim, 2013). The retina's projection to the superior colliculus (SC) has served as a model to understand the molecular and activity-dependent forces that drive map formation

*Corresponding Author: Jason Triplett, PhD, Assistant Professor, Center for Neuroscience Research, Children's National Medical Center, 111 Michigan Ave, NW M7632, Washington, DC 20010, 202-476-3985, jtriplett@childrensnational.org.

AUTHOR CONTRIBUTIONS

M.T.O. helped design the study, conducted the intrinsic signal optical imaging and *in silico* modeling experiments, and wrote the initial draft of the manuscript. D.A.F. helped design the study, provided financial support for salaries and supplies, and helped edit the manuscript. M.P.S. designed the study, provided financial support for salaries and supplies, wrote and edited the manuscript. J.W.T. helped design the study, conducted the axon tracing experiments, provided support for salaries and supplies, wrote and edited the manuscript.

for decades (Gaze, 1981). Retinal ganglion cells (RGCs) project to the SC during early postnatal life and are refined to a final topographic map by the end of the first postnatal week (Mclaughlin et al., 2003). Graded molecular cues play a role in the establishment of retinocollicular topography along the azimuth axis. Specifically, EphA receptor tyrosine kinases and their ligands, the ephrin-As, are expressed in counter gradients along the temporal-nasal (T-N) axis of the retina and the anterior-posterior (A-P) axis of the SC. Interactions between innervating RGCs and collicular cells results in temporal RGCs terminating anteriorly, while nasal RGCs terminate posteriorly, in the SC (Triplett, 2014). Disruption of EphA/ephrin-A signaling results in topographic errors along the azimuth axis in the SC, dorsal lateral geniculate nucleus (dLGN) and primary visual cortex (V1) that manifest anatomically as ectopic termination zones (TZs) and functionally as topographically incorrect receptive fields (Brown et al., 2000; Cang et al., 2005a; 2008b; Feldheim et al., 2000; Frisén et al., 1998; Pfeiffenberger et al., 2006; Triplett et al., 2009).

In addition to molecular cues, correlated neuronal activity plays a critical role in map formation. During development, spontaneous waves of activity propagate across the retina and initiate corresponding waves in retinorecipient nuclei (Ackman et al., 2012; Meister et al., 1991). Disruption of these waves results in errors in topography, such that the TZs of RGCs in the SC are found in approximately the correct topographic location, but fail to refine to establish a discrete map (Chandrasekaran et al., 2005; Mclaughlin et al., 2003). Functionally, this is reflected as an increase in the number of RGC synaptic inputs to collicular cells and increases in the receptive field properties of these neurons (Cang et al., 2008a; Chandrasekaran et al., 2005). Interestingly, anatomical and functional perturbations in the absence of spontaneous activity are observed specifically in the azimuth domain, which has been attributed to the unique spatiotemporal properties of retinal waves (Stafford et al., 2009). Similar changes are also observed in the dLGN and V1, suggesting a common role for spontaneous activity in topographic map formation throughout the visual system (Cang et al., 2005b; Grubb et al., 2003). Together, molecular- and activity-dependent forces play the dominant roles in topographic mapping along the azimuth axis, as disruption of both forces simultaneously results in a nearly complete loss of topography in the SC (Cang et al., 2008b; Pfeiffenberger et al., 2006). However, the relative strength of each of these forces remains unclear.

Based on *in vivo* studies in genetically-modified mice, several computational models have been developed to explain the role of molecular- and activity-dependent forces in the establishment of topography. The relative signaling model argues that local comparisons in EphA signaling strength by RGCs results in an ordered distribution of terminals in the SC (Reber et al., 2004; Bevins et al., 2011). Such a model is supported by experiments in which the level of EphA receptor signaling was altered in a subset of RGCs, resulting in the formation of a bifurcated map in the SC (Brown et al., 2000). A second, permissive arborization model posits that map development proceeds in a step-wise fashion, in which molecular forces establish broad zones for potential synapse formation, while later activity-dependent and competitive forces dictate final map organization (Grimbert and Cang, 2012). This model is supported by accumulating evidence of a role for EphA/ephrin-A reverse signaling (Lim et al., 2008; Rashid et al., 2005; Yates et al., 2001), axonal competition

(Triplett et al., 2011) and interaxonal signaling (Suetterlin and Drescher, 2014) in retinocollicular map formation. Finally, stochastic models proposes that RGCs exchange synapses in the SC to optimize adhesion, driven by a combination of molecular forces, competition and activity (Koulakov and Tsigankov, 2004; Tsigankov and Koulakov, 2006; 2010). While this model replicates topographic organizations found in control and mutant mice *in vivo*, clear empirical data supporting stochasticity remains elusive.

Here, we demonstrate an activity-dependent, stochastic mechanism for the establishment of retinocollicular topography. Utilizing intrinsic signal optical imaging in heterozygous *Islet2-EphA3* knock-in mice ($Isl2^{EphA3/+}$), we show that map organization exhibits tremendous heterogeneity both among $Isl2^{EphA3/+}$ individuals and even within single animals. Map heterogeneity is also exhibited anatomically, as assayed by anterograde tracing of RGCs and analysis of $Isl2^{+}$ RGC projection patterns. Neural activity is required for the manifestation of heterogeneity in map organization, since disruption of spontaneous retinal waves resulted in only a single type of map. Heterogeneity akin to that observed in the $Isl2^{EphA3/+}$ was replicated by a computational model when the EphA signaling factor was set appropriately. Small variations in this factor resulted in consistent map organizations, mimicking the consistency found in wild type (WT) and homozygous $Isl2^{EphA3/EphA3}$ animals. Taken together, these results suggest that activity-dependent and molecular forces are nearly equal in balance during the establishment of topography and that local topography can be driven by either in a stochastic manner.

RESULTS

Heterogeneity of map organization in $Isl2^{EphA3/+}$ mice

One of the most elegant investigations of the role of EphA signaling in topographic map formation involved the generation of the *Islet2-EphA3* knock-in mouse line ($Isl2^{EphA3}$) (Brown et al., 2000). In these mice, an EphA3 cDNA was inserted into the 3' untranslated region of the *Islet2* locus. This manipulation produced a salt and pepper arrangement of two populations of RGCs: 1) $Isl2^{-}$ RGCs that express endogenous levels of EphA receptors and 2) $Isl2^{+}$ RGCs that express endogenous EphAs and exogenous EphA3. In homozygous $Isl2^{EphA3/EphA3}$ mice, the difference in total EphA signaling between $Isl2^{-}$ and $Isl2^{+}$ RGCs is large, resulting in the segregation of these two populations in the SC and the formation of two coherent anatomical and functional maps of space (Brown et al., 2000; Triplett et al., 2009). In heterozygous $Isl2^{EphA3/+}$ mice, however, the difference in EphA signaling strength between populations of $Isl2^{+}$ and $Isl2^{-}$ RGCs varies depending on their location along the T–N axis of the retina. For instance, in nasal retina, expression of endogenous EphAs is low, so $Isl2^{+}$, EphA3-overexpressing RGCs should have distinct EphA signaling strengths from $Isl2^{-}$ RGCs. In contrast, RGCs in the temporal retina express high levels of endogenous EphAs, such that the difference in EphA signaling strength is minimal between $Isl2^{+}$ and $Isl2^{-}$ RGCs. Thus, one prediction of this pattern of EphA expression would be that $Isl2^{+}$ and $Isl2^{-}$ RGCs from the nasal retina would project to two distinct regions of the SC, while those from the temporal retina would project to a similar region in the anterior SC. Indeed, anatomical tracing experiments in $Isl2^{EphA3/+}$ mice supported this hypothesis (Brown et al., 2000). These data also predict that the azimuth representation along the A–P axis of the SC

would be split into two incomplete maps of space, wherein the anterior ~2/3 of the map would have a full representation of central visual space and a partial representation of the periphery, while the posterior 1/3 would have a partial representation of the periphery. However, the functional organization in that SC in Isl2$^{EphA3/+}$ mice has not been investigated.

To determine the functional topographic organization of the SC in adult Isl2$^{EphA3/+}$ mice, we performed intrinsic signal optical imaging, as described previously (Kalatsky and Stryker, 2003). This technique allows the observation of either the azimuth or elevation representation of space at a population level in a large portion of the SC at once. Indeed, in WT mice, a single azimuth representation and single elevation representation are observed in the SC contralateral to the stimulated eye (Figure 1D–E). In adult homozygous Isl2$^{EphA3/EphA3}$ mice, the azimuth representation in the SC is duplicated, while the elevation representation remains singular, consistent with our previous findings (Figure 1F–G) (Triplett et al., 2009). Interestingly, while heterozygous Isl2$^{EphA3/+}$ animals had functional maps of similar size and strength to WT and Isl2$^{EphA3/EphA3}$ mice (Figure S1A–C), we observed heterogeneity in the organization of azimuth representations (Figure 1H–O, n = 16). These representations fell into three qualitative categories: 1) single (Figure 1H), similar to those of WT animals, 2) doubled (Figure 1J), similar to those seen in Isl2$^{EphA3/EphA3}$ mice, and 3) partially doubled and partially single (Figure 1L), hereafter referred to as mixed-type. Importantly, the differences observed were not due to variability in responsiveness, as each of the types occupied similar areas of the SC (Figure S1D).

To quantitatively categorize azimuth map organizations in Isl2$^{EphA3/+}$ mice, we plotted the azimuth phase as a function of position along the A–P axis at three different isoelevation points in the map (Figure 1N). We then determined two indices to better describe the relationships between the azimuth representations at these distinct elevations (see Materials and Methods). Briefly, we first generated a “linear fit index,” which describes the goodness of fit to a linear regression for the azimuth phase plot at each elevation measured. Next, we determined an “intramap correlation index,” which describes the fidelity of map organization between each azimuth phase plot within a single map. By plotting the linear fit index as a function of the intramap correlation index, we found that individual maps fell into distinct clusters, corresponding to single maps of Isl2$^{+/+}$ mice, double maps of Isl2$^{EphA3/EphA3}$ mice, and mixed maps of Isl2$^{EphA3/+}$ which fell between the single and double clusters (Figure 1O). Based on this analysis, we found that 25.0% (4/16) of Isl2$^{EphA3/+}$ maps were single, 18.8% (3/16) were double and 56.3% (9/16) were mixed type.

Although the maps of azimuth display the most obvious differences, the elevation maps differ as well. In Isl2$^{EphA3/EphA3}$ mice, the elevation maps display a discontinuity that allows each of the maps of space to be coherent (Figure 1G and (Triplett et al., 2009)). This discontinuity is present only in the mice that have doubled or partially doubled maps of azimuth and is absent in the Isl2$^{EphA3/+}$ mice with single maps (Figure 1M). Taken together, these data demonstrate heterogeneity in the organization of maps in the Isl2$^{EphA3/+}$ SC and suggests a stochastic process may underlie map formation.

Heterogeneity of map organization in Isl2$^{EphA3/+}$ mice is not due to genetic variation

One potential source of heterogeneity in map organization observed in Isl2$^{EphA3/+}$ mice could be differences in genetic background between mice. If this were the case, then the organization of the visual map should be the same in both colliculi of an individual mouse. To determine if this were the case, we imaged the colliculi of both hemispheres in several Isl2$^{EphA3/+}$ mice. Strikingly, we often found different azimuth representations in the right and left SCs in Isl2$^{EphA3/+}$ mice in which both colliculi were imaged (Figure 2B & C). Indeed, we found that in 5 of 7 mice, the organization of maps in the left and right SC fell into distinct categories when plotting the linear fit index as a function of the intramap correlation index (Figure 2D). For example, Figure 2C depicts an Isl2$^{EphA3/+}$ animal in which the azimuth representation was singular in the right hemisphere, but mixed type in the left hemisphere. These data suggest that heterogeneity in map organization is not due to subtle changes in EphA3 expression level due to genetic background. Despite this, the possibility remains that subtle differences in EphA3 expression from the Isl2 locus between eyes may cause the heterogeneity observed between colliculi of the same animal. However, our observations that different regions of a single SC are organized differently in a substantial portion of Isl2$^{EphA3/+}$ mice, suggests that genetic differences play a minimal role in the heterogeneity observed.

Heterogeneity of map organization in Isl2$^{EphA3/+}$ mice is not due to suppression of visual responses

Another possible explanation for the heterogeneity observed in individual functional maps, is that some of the retinal inputs into the SC are being functionally suppressed. Visual maps in primary visual cortex are able to suppress aberrant input from the lateral geniculate nucleus in the “Midwestern” variety of Siamese cat (Kaas and Guillery, 1973), but the extent to which maps in SC can suppress retinal input is unknown. To address the possibility of functional suppression, we imaged the SCs of Isl2$^{EphA3/+}$ mice while showing them spatially-restricted stimuli. These stimuli would only excite a small part of the retina at once, potentially activating ectopic termination sites that are normally suppressed when full-field stimuli are presented. We focused on Isl2$^{EphA3/+}$ mice with mixed-type maps, since we would be able to compare in the same SC areas of activation that give a doubled map and areas of activation that give a single map. Isl2$^{EphA3/+}$ mice were shown a series of stimuli consisting of short bars that subtended only 5° of visual angle in azimuth (Figure 3B). The areas in SC that each bar activated were combined, and this map was compared to the map derived from conventional full-field stimuli (Figure 3C–F). In every case (n = 4), the map obtained from spatially-restricted stimuli matched the maps obtained with full-field stimulation very well. These results confirm the reliability of our imaging method and do not support functional suppression as the source of heterogeneity observed in Isl2$^{EphA3/+}$ mice.

Functional heterogeneity of map organization in Isl2$^{Eph\ A3/+}$ mice reflects anatomical heterogeneity

Another possible interpretation of these data is that the heterogeneity in the organization of intrinsic optical signal maps reflects alterations in collicular neuron functionality rather than altered projection patterns of RGCs. As an initial test of this possibility, we examined the

projection patterns of Isl2^{+} RGCs using a transgenic mouse in which GFP is expressed in the soma, dendrites and axons (Triplett et al., 2014). Consistent with our functional data, we observed heterogeneity in the organization of Isl2-GFP^{+} RGC projections in the SC of Isl2$^{EphA3/+}$ mice (Fig. 4). As expected, we found the densest Isl2-GFP^{+} innervation in the anterior SC and a readily observable "boundary," presumably at the border of a duplicated map (Figure 4A, dotted line in A' & A"). Interestingly, the shape and precise location of this "boundary" varied between colliculi of different mice and between collicular hemispheres of the same mouse (Figure 4A' vs. A"). Posterior to the "boundary" we observed the greatest degree of heterogeneity. In some colliculi, Isl2-GFP^{+} RGCs appeared to be evenly distributed over the posterior SC (Figure 4A, right hemisphere), while in others, large regions appeared devoid of Isl2-GFP^{+} RGC innervation (Figure 4A, left hemisphere & Figure 4C). In several instances we observed dense islands of Isl2-GFP^{+} innervation (Figure 4A, A' & A", arrows), suggesting that clustering of these terminals occurs in a stochastic manner. To quantitatively asses the heterogeneity of Isl2-GFP^{+} RGCs projections in the SC of Isl2$^{EphA3/+}$ mice, we compared the intensity of GFP^{+} terminals along the A–P axis at three positions along the M–L axis (Figure 4C & D, bottom row). As a control, we measured the intensity along the same M–L positions of all RGC terminals, which were labeled by intraocular injection of fluorescently-tagged Cholera Toxin subunit B (Figure 4B and D, top row). Plotting fluorescence intensity as a function of the position along the A–P axis, we found that the distribution of all RGCs was similar at each M–L position across colliculi (Figure 4D, top row). In contrast the distribution of Isl2-GFP^{+} terminals showed more variability (Figure 4D, bottom row). To quantify this, we calculated the pairwise correlation coefficients between intensity plots for both Isl2-GFP^{+} and all RGCs for each SC and determined the average to generate a correlation index (n = 9 SCs for all RGCs and n = 12 SCs for Isl2-GFP^{+} RGCs). We found that at each M–L position, the correlation index of Isl2-GFP^{+} RGC projections was significantly reduced compared to that of all RGCs (Figure 4E). These data demonstrate heterogeneity in the projection patterns of Isl2-GFP^{+} RGC subtypes in Isl2$^{EphA3/+}$ mice.

To further analyze possible variation in the anatomical organization in Isl2$^{EphA3/+}$ mice, we traced RGC projections by focal injection of DiI into the nasal retina, since the posterior SC is where the observed heterogeneity is expressed functionally. In contrast to previous reports (Bevins et al., 2011; Brown et al., 2000; Reber et al., 2004), we found that labeled nasal axons in Isl2$^{EphA3/+}$ mice exhibited variability in the organization of their terminations (Figure 5). Consistent with previous studies, we found that a single injection in nasal retina of adult Isl2$^{EphA3/+}$ mice resulted in two termination zones (TZs) in the SC (55.6%, 10/18) (Figure 5A & G); however, in a substantial proportion of cases, a single injection in nasal retina resulted in one TZ (33.3%, 6/18) or a "smeared" TZ (11.1%, 2/18) (Figure 5A–C). In addition to examining the TZ pattern of labeled RGCs in these mice, we also performed intrinsic signal optical imaging in the SC of the same mouse in order to make direct comparisons of anatomical and functional organizations. As expected, functional map organizations reflected anatomical organizations on the whole. Indeed, a χ^2 test in which single maps were assigned an expected value of 1 TZ, double maps 2 TZs and mixed map 1.5 TZs, the probability of observing the expected number of TZs is very high (χ^2_{single} = 0.963, χ^2_{double} = 0.987, χ^2_{mixed} = 0.975). These data suggest that the anatomical

organization of nasal RGC inputs in the SC of Isl2$^{EphA3/+}$ mice are heterogeneously organized in a similar manner to that observed for the functional representation.

Spontaneous retinal activity required for heterogeneity

Our findings thus far suggest that EphA signaling in Isl2$^{EphA3/+}$ mice is at a level that produces instability and heterogeneity in map organization in the posterior SC. Several lines of evidence suggest that ephrin-A/EphA molecular interactions provide a force that would drive map organization to a duplicated state in the Isl2$^{EphA3/+}$SC; thus, a counterbalancing force of equal magnitude must exist in the developing SC to drive map organization to the single and mixed-type states. One possible counter-balancing force is correlated spontaneous retinal waves during early post-natal development, which have been shown to play a critical role in topographic mapping, acting to cluster axonal terminals of neighboring RGCs and refine the receptive fields of individual collicular neurons (Chandrasekaran et al., 2005; Mclaughlin et al., 2003). We hypothesized that the correlated activity generated by spontaneous waves provides a counter-balancing force strong enough to overcome the ephrin-A/EphA molecular force in the Isl2$^{EphA3/+}$SC. To test this possibility, we imaged the SCs of mice in which the normal pattern of spontaneous retinal waves were disrupted. In mice lacking the β2 subunit of the nicotinic acetylcholine receptor (β2$^{-/-}$), retinal waves have altered spatiotemporal properties, resulting in abnormal topographic refinement in the SC (Chandrasekaran et al., 2005; Mclaughlin et al., 2003; Stafford et al., 2009). We crossed Isl2$^{EphA3/+}$ mice into the β2$^{-/-}$background to determine the role of spontaneous retinal waves in the generation of heterogeneity in topographic organization. While we found that both the azimuth and elevation representations of Isl2$^{EphA3/+}$/ β2$^{-/-}$ mice had significantly decreased peak amplitudes in comparison to those of Isl2$^{EphA3/+}$/ β2$^{+/-}$ littermates (Figure S2), we were able to obtain interpretable maps (Figure 6). In support of our hypothesis, we found that the in Isl2$^{EphA3/+}$/ β2$^{-/-}$ mice, retinocollicular maps were similar across SCs, all resembling single maps both qualitatively and quantitatively (Fig. 6B, E & F). This surprising result may be explained by the known alterations in spatiotemporal properties of waves in the β2$^{-/-}$ mouse (Stafford et al., 2009; see Discussion). Importantly, heterogeneity remained in Isl2$^{EphA3/+}$/ β2$^{+/-}$ littermates exhibited map heterogeneity maps, as 50.0% (2/4) had single maps and 50.0% (2/4) had mixed-type maps (Figure 6A & F). Taken together, these data suggest that correlated spontaneous retinal activity acts as a counterbalance to molecular forces to influence the local organization of the retinocollicular map.

In silico model predicts map heterogeneity of map organization in Isl2$^{EphA3/+}$ mice

The presence of mixed-type maps and heterogeneity observed in Isl2$^{EphA3/+}$ mice suggests a stochastic process in map formation driven by interactions between molecular-and activity-dependent forces. However, neither experimental nor modeling studies have revealed this possibility. Indeed, previous computational modeling of SC development has been used to validate the results of anatomical tracing in Isl2$^{EphA3/EphA3}$ and Isl2$^{EphA3/+}$ mice (Bevins et al., 2011; Grimbert and Cang, 2012; Koulakov and Tsigankov, 2004; Tsigankov and Koulakov, 2010). Here, we modify a previously described mathematical model to replicate *in silico* the variability we observed *in vivo*. In our model, we assume that all RGCs initially project to the posterior-most SC, regardless of their cell body location along the T–N axis of the retina, as previously described (Simon and O'Leary, 1992). Indeed, this is necessary for

a stochastic resolution to the push and pull forces of activity and molecules we observe in $Isl2^{EphA3/+}$ mice. However, recent models have suggested that in the $Isl2^{EphA3/+}$ and $Isl2^{EphA3/EphA3}$ mouse models, $Isl2^{+}$ RGCs are unable to project to the posterior-most SC due to the high expression level of EphA receptors (Grimbert and Cang, 2012). To resolve this issue, we examined Isl2-GFP^{+} RGC projection patterns during the development of retinocollicular topography. In contrast to previous models, we find Isl2-GFP^{+} fibers in the posterior-most SC at early developmental ages (postnatal day 2 and 4 (P2 and P4)) in $Isl2^{EphA3/+}$ mice (Figure S3A & B). Indeed, even at ages in which refinement has begun and Isl2-GFP^{+} fibers show a concentration in the anterior SC (P6 & P8), a subset of fibers can be found in the posterior SC (Figure S3C & D). Taken together with our modeling results, these data suggest that $Isl2^{+}$ and Isl2− RGC axons are intermingled during development of retinocollicular topography in $Isl2^{EphA3/+}$ mice, allowing for a competition between molecular and activity-dependent forces that resolves itself in a stochastic manner.

To better describe the stochastic nature of topographic map formation, we modified the model proposed by Tsigankov and Koulakov, in which map formation depends on graded chemical cues and activity-dependent refinement (Tsigankov and Koulakov, 2006; 2010). The SC is represented by a 100 by 100 matrix to simulate the termination sites for RGC axons (Fig. 7A). The chemical cues along the N–T axis of the map simulate the graded expression of EphA and ephrin-A in both retina and SC (see Materials and Methods for detailed descriptions). The exogenous EphA3 in the retinas of $Isl2^{EphA3/EphA3}$ and $Isl2^{EphA3/+}$ mice is simulated by adding a fixed factor, ΔR, to the “chemical cue” profile of every other RGC; the ΔR used for modeling $Isl2^{EphA3/EphA3}$ mice is twice as much the one used to model $Isl2^{EphA3/+}$ mice to represent the effect of possessing two *Isl2-EphA3* alleles as opposed to one. Initially, the map is random, but it undergoes a series of optimization steps. At each step, two randomly chosen RGCs are exchanged with the probability $p = 1/[1 + \exp(4*\Delta E)]$, where $\Delta E = \Delta E_{chem} + \Delta E_{act}$ is the change in adhesive energy due to the exchange. In general, ΔE_{chem} is minimized when the RGC expressing the highest amounts of receptor project to places in the SC expressing the lowest amounts of ligand and *vice versa*, which makes sense given the repulsive nature of the interaction between the EphAs and ephrin-As. ΔE_{act} is minimized when RGCs that are close to each other in the retina project close to each other in the SC. After 10^7 steps, orderly and organized topographic maps appear. When ΔR is set to zero, simulating map formation in WT animals, the maps are always single (Fig. 7B). When ΔR is set to a high number (0.70), representing conditions in the $Isl2^{EphA3/EphA3}$ mouse, the maps are always doubled (Fig. 7C). However, at the intermediate value of ΔR=0.35, different simulation runs give maps of divergent structures, reminiscent of the maps seen in $Isl2^{EphA3/+}$ mice (Fig. 7D). Some runs give rise to maps that are almost entirely single, or doubled, and the majority of maps are mixed.

Previous studies of topographic map formation hint that changes in the sum of EphA in the retina results in alterations of retinocollicular map organization (Bevins et al., 2011; Reber et al., 2004). To determine the sensitivity of our optimality model, we varied the value of ΔR around the intermediate value that resulted in heterogenous outcomes. We found that increasing or decreasing the value of ΔR by +/ −0.05 (+/−16.6%) eliminated heterogeneity and consistently resulted in fully doubled or single maps, respectively (Figure 7E). These

data indicate that the *in silico* model utilized here is able to replicate key aspects of map formation, including the heterogeneity observed *in vivo* in Isl2$^{EphA3/+}$ mice. Further, the sensitivity of map organization to small changes in ΔR taken together with our finding that spontaneous retinal activity is required for heterogeneity provide strong support that molecular- and activity-dependent forces are nearly equally in balance during the formation of topographic maps.

DISCUSSION

The retinocollicular projection has served as a model to understand the mechanisms by which topographic projections between brain regions are established. Important roles for both molecular cues and activity-dependent forces have been well established, yet how these forces interact to mediate map formation remains unresolved. Here we demonstrate that local topographic map formation proceeds stochastically, driven by equally-balanced molecular- and activity-dependent forces. These findings not only resolve the issue of the relative roles of molecular cues and activity in the establishment of topography, but also show a novel stochasticity in the establishment of retinocollicular connectivity.

Heterogeneity of retinocollicular map organization in Isl2$^{EphA3/+}$ heterozygous knock-in mice

Previous investigations of retinocollicular mapping in the Isl2^{EphA3} knock-in mice pointed towards a relative signaling model of map formation. In heterozygous Isl2$^{EphA3/+}$ mice, anatomical tracing suggested that Isl2^{+} and Isl2− RGCs originating in the nasal retina projected to distinct locations in the posterior SC, while those from temporal retina “collapsed” into a single map (Brown et al., 2000). Indeed, elegant experiments manipulating the expression level of other retinal EphA receptors confirm this model, and mathematical models were derived to describe these data and predict other findings (Bevins et al., 2011; Reber et al., 2004). In contrast, our functional experiments reveal extensive heterogeneity in the organization of retinal inputs to the SC in Isl2$^{EphA3/+}$ mice. One potential explanation of this difference is that the anatomical tracings in previous studies can only sample a small portion of the map at a time, while our functional imaging technique allows us to monitor map organization as a whole. Thus, examining map organization at a population level may reveal heterogeneity that anatomical tracing experiments could not. However, we found significant heterogeneity in the anatomical projection pattern of DiIlabeled nasal RGCs in Isl2$^{EphA3/+}$ mice that were consistent with the heterogeneous functional organization of the collicular map. In 33.3% (6/18) of Isl2$^{EphA3/+}$ animals in which we traced nasal RGCs, there was a single TZ in the SC, whereas previous studies reported that all nasal tracings resulted in two TZs. Such a discrepancy may be due to the small number of tracings carried out in previous studies; only 5 were done in the nasal retina (defined as ≤ 40% of the N–T axis) (Brown et al., 2000). In other studies, tracings of nasal RGCs in Isl2$^{EphA3/+}$ mice with altered EphA4 or EphA5 levels consistently showed two termination zones (Bevins et al., 2011; Reber et al., 2004). However, as the mathematical model we propose here suggests, altering the sum of the EphA signaling force even slightly can have dramatic effects on the consistency of the organization of the resulting collicular map.

In addition to the heterogeneity of map organizations between colliculi of ls2$^{EphA3/+}$ mice, the presence of mixed-type maps challenges current models of map formation. Importantly, to our knowledge, neither the relative signaling nor the permissive arborization models predict the presence of either heterogeneous map organizations between Isl2$^{EphA3/+}$ SC or multiple map organizations within a single SC. In contrast, the stochastic optimization model presented here is able to replicate not only the heterogeneity of map organizations observed in the Isl2$^{EphA3/+}$ SC, but also mixed-type map organizations in a single SC. This is an important distinction, as the observation of mixed-type maps in the Isl2$^{EphA3/+}$ SC suggests that the forces of molecular cues and spontaneous activity are nearly equally in balance, and that the local organization of retinal inputs is determined stochastically. Incorporating this novel aspect into future models of retinocollicular map formation is a necessary step towards the development of accurate computational simulations.

Activity-dependent forces, rather than genetic modifiers, drive heterogeneity

Our mathematical model of map formation revealed that subtle changes in the expression level of EphAs results in dramatic changes in the organization of the retinocollicular map in Isl2$^{EphA3/+}$ mice. A parsimonious explanation of the heterogeneity of map organization observed in Isl2$^{EphA3/+}$ mice, then, would be that differences in the genetic background may affect EphA3 expression. Three critical observations are inconsistent with this explanation of map heterogeneity. First, we observed several instances in which the functional organization of the collicular map in one hemisphere differed significantly from that of the contralateral hemisphere in a single mouse. Second, this bilateral difference was also observed in the projection patterns of genetically-labelled Isl2^{+} RGCs. Third, we found that disruption of Stage 2 spontaneous retinal waves eliminated map heterogeneity in Isl2$^{EphA3/+}$ mice. Taken together, these findings reduce the possibility that subtle differences of expression in EphA3 due to alterations in the expression or efficacy of genetic modifiers in driving map heterogeneity.

These findings also point to an instructive role for retinal waves in the establishment of retinocollicular topography. Previous work from several labs has established that Stage 2 cholinergic waves play a critical role in the refinement of retinocollicular projections (Chandrasekaran et al., 2005; Mclaughlin et al., 2003; Pfeiffenberger et al., 2006). However, the majority of topographic guidance of RGCs is thought to be mediated by graded molecular cues. Here, we show that retinal waves can play an instructional role in the local organization of the retinocollicular map, resulting in dramatic rearrangements distinct from those predicted by the local relative signaling and permissive arborization models previously proposed. The instructive nature of these waves has previously been demonstrated for the alignment of visual topographic maps of space in the SC (Triplett et al., 2009) and the migration of interneurons in the dorsal lateral geniculate nucleus (Golding et al., 2014). However, the specific mechanisms by which these waves are able to mediate such instruction remain unclear.

Based on previous studies, we predicted that in Isl2$^{EphA3/+}$ mice, molecular forces would drive the map towards a duplicated state, while spontaneous retinal waves would drive the map towards a singular organization. In contrast, we found that the azimuth representations

in Isl2$^{EphA3/+}$ mice in the absence of correlated spontaneous retinal activity were organized into a single map. One potential explanation for this surprising result relates to the spatiotemporal properties of retinal waves in the WT and β2$^{-/-}$ situation. First, retinal waves in the β2$^{-/-}$ are present, although they occur less frequently, travel more quickly and correlate the activity of a more widely dispersed population of RGCs. These unique changes in wave properties may actually confer the ability of waves to better overcome the molecular forces that would drive the Isl2$^{EphA3/+}$map to a duplicated state, instead grouping larger populations of RGCs into a single map organization. Alternatively, disruption of the normal pattern of spontaneous activity could interfere with the ability of RGCs to respond to ephrin-A molecular cues in the SC (Nicol et al., 2007). In this case, RGCs in the Isl2$^{EphA3/+}$ mouse would be guided to a rough, singular topographic map through alternative molecular cues or axon-axon interactions. However, we do not favor this interpretation, since the SC of Isl2$^{EphA3/EphA3}$/β2$^{-/-}$ was still able to organize into a duplicated state along the azimuth axis (Triplett et al., 2009).

What purpose might stochasticity serve in the establishment of topographic maps in the visual system? On the surface, such a mechanism would introduce the potentially costly consequence of poor fidelity in transfer of spatial information between visual centers. Indeed, previous studies in the human and non-human primate LGN revealed variation in laminar organization, which was presumed to allow for preservation of retinotopy (Hickey and Guillery, 1979; Kaas et al., 1978). And, in ferrets in which eye-specific lamination in the LGN was disrupted by activity blockade, retinotopy was preserved (Huberman et al., 2002). In contrast, it was recently reported that domains of the mouse SC preferring distinct orientations are maintained at the expense of local topography (Feinberg and Meister, 2015). Thus, stochasticity may allow flexibility in the development of precise topography at local levels in order to facilitate the establishment of parallel visual circuits, or *vice versa*. Indeed, these ideas have previously been discussed in relation to the monkey LGN (Lee and Malpeli, 1994; Stryker, 1994), suggesting these mechanisms may be utilized in other areas of the visual system.

Stochastic model of retinocollicular mapping

The unexpected heterogeneity of map organization in the Isl2$^{EphA3/+}$ SC that we report here requires a rethinking of previously described models of retinocollicular map formation. For instance, the relative signaling model for mapping along the A–P axis of the SC relies heavily upon forces derived from graded molecular cues (Reber et al., 2004). This model predicts that large differences in EphA receptor signaling strength, as in Isl2^{+} and Isl2^{-} neurons from the nasal retina of Isl2$^{EphA3/+}$ mice, would result in the formation of two distinct termination zones in the posterior half of the SC. Our data demonstrate that in a substantial proportion of Isl2$^{EphA3/+}$ mice, the nasal portion of the retinocollicular map in the SC is not completely duplicated, suggesting the relative signaling model cannot explain the mechanisms of mapping in totality. In contrast to the relative signaling model, a recent permissive signaling model proposes a less prominent role for molecular cue-derived forces in guiding topographic maps (Grimbert and Cang, 2012). In this model, secondary stages of Hebbian plasticity and competition for limiting resources drive the majority of topographic map formation. Consistent with some of our empirical data, the permissive signaling model

predicts a retinocollicular map that is not completely duplicated in the posterior SC of Isl2$^{EphA3/+}$ mice. However, this model did not predict the heterogeneity between colliculi that we observed with functional imaging and anatomical tracing, suggesting that this model may not completely account for all the mechanisms of topographic map formation.

In contrast to previous models, the *in silico* model proposed here replicates the heterogeneity observed *in vivo*. This optimality model builds on a previously described framework (Tsigankov and Koulakov, 2010; 2006), which takes into account molecular forces along both the A–P and M–L axes of the SC, as well as correlated activity. A third factor, ΔR, representing the additional EphA3 receptor expression in Isl2^{+} cells, allowed us to mimic magnitude of ephrin-A/ephA signaling in WT, Isl2$^{EphA3/+}$ and Isl2$^{EphA3/EphA3}$ mice. When ΔR is at a minimum or maximum, the model predicts map organization that is singular or doubled, respectively. At intermediate levels, heterogeneity if map organization is predicted. We found that slight variations in ΔR around the intermediate level yielded substantial differences in the organization and heterogeneity of predicted maps. Such sensitivity to small differences in ΔR, suggests a simultaneous interaction between molecular- and activity-dependent forces, rather than a molecularly-driven large-scale map formation that is refined at finer scale by activity-dependent mechanisms. Interestingly, both the relative signaling and permissive arborization models also include a factor to account for the added EphA3 expression in Isl2^{+} cells, and it would be informative to vary this factor in those models to determine if they are then able to replicate the heterogeneity observed here.

Relative strengths of molecular cues and spontaneous activity in map formation

Under normal developmental circumstances, molecular and activity-dependent forces act in concert to instruct the formation of an orderly topographic map. Previous studies in which one force or the other was completely disrupted revealed the importance of each in topographic mapping but could not address the relative strengths of the two. In the Isl2$^{EphA3/+}$ mouse, both of these forces remain intact, but they are no longer acting completely in concert. We show here, that when these forces in opposition are nearly equally strong, map organization is heterogeneous, indicating that it is determined in a stochastic manner. Such stochasticity was particularly dramatic in mixed type maps, where one portion of the SC is organized following molecular instructions, while in another portion activity-dependent forces drive mapping. These findings provide powerful evidence that a similar push-pull of molecular and activity-dependent forces drives map formation in normal development.

EXPERIMENTAL PROCEDURES

Mice

Isl2-EphA3 knock-in, *nAChR-β2*, and Isl2-GFP mutant mice were generated and genotyped as previously described (Brown et al., 2000; Triplett et al., 2014; Xu et al., 1999). Mice were maintained on a mixed CD-1/C57Bl6 background. All mouse protocols were performed in accordance with the University of California, Santa Cruz, University of California, San Francisco, and Children's National Health System IACUC standards.

Functional imaging

Imaging of intrinsic optical signals was performed as described previously (Cang et al., 2008b; Kalatsky and Stryker, 2003). Briefly, adult mice (>P40) were anesthetized with urethane (1.0 g/kg in 10% saline solution) supplemented with chlorprothixene (0.03 mg/kg). Animals were also given atropine (0.3 mg/kg) and dexamethasone (2 mg/kg). A tracheotomy was performed, and a craniotomy was made along the midline and lambda sutures of the left hemisphere. The cortex overlying the SC was aspirated, and we imaged maps of the SC. Optical images of the cortical intrinsic signal were obtained at the wavelength of 610 nm, using a Dalsa 1M30 CCD camera (Dalsa, Waterloo, Canada) controlled by custom software. A high refresh rate monitor (Nokia Multigraph 4453, 1024 × 768 pixels at 120 Hz) was placed 25 cm away from the animal where it subtended 70° of the contralateral visual field. Drifting thin bars (2° width) were displayed on the monitor. Most experiments used bars the length of the full screen, but some experiments used shorter bars the length of 5° of visual angle. Animals were presented with horizontal or vertical bars drifting orthogonal to the axis corresponding to either the dorsal-ventral or nasal-temporal axis of the animal in order to stimulate constant lines of elevation or azimuth, respectively. In some cases, an additional craniotomy was made on the right side to image the other SC.

Quantitative analysis of functional imaging

The peak amplitude of maps was measured directly. The size of topographic maps were analyzed using custom software in Matlab. Size was taken to be the response area of the elevation map within 15% of the peak magnitude. To quantify the organization of azimuth maps, we first plotted azimuth phase as a function position along the A–P axis at three isoelevation points (−25°, 0° and 25°). A “linear fit index” was calculated as the ratio $(R^2_{max} - R^2_{min})/(R^2_{max} + R^2_{min})$, where R^2_{max} and R^2_{min} were the highest and lowest coefficient of determination values to a linear regression among the three azimuth phase plots for each map, respectively. An “intramap correlation index” was calculated by œ $\log((CC_{-25:0} + CC_{0:25} + CC_{-25:25})/3)$ where $CC_{-25:0}$, $CC_{0:25}$ and $CC_{-25:25}$ were the pairwise correlation coefficients between the three azimuth phase plots for each map, determined using the “CORREL” function in Excel (Microsoft, Seattle).

Axon tracing and fluorescent microscopy

For focal tracing of retinal projections adult mice were anaesthetized by intraperitoneal injection of 100 mg/kg ketamine and 10 mg/kg xylazine. A small amount of 1,1’-dioctadecyl-3,3,3’,3’-tetramethylindocarbocyanine (DiI) (Invitrogen, Carlsbad) was injected at focal regions intraocularly using a handheld picospritzer (Parker Instrumentation, Cleveland) and a pulled glass needle as described previously (Feldheim et al., 2000). Between one and two weeks after injection, animals were functionally imaged as described above. After imaging, animals were immediately sacrificed and intracardially perfused with ice-cold 4% paraformaldehyde (PFA) in PBS. Brains were dissected out and fixed overnight. Fluorescent imaging of termination zones was performed in whole mount using a digital camera through a 1.25X objective on a BX61 Fluorescent microscope (Olympus). Fluorescent images were obtained blindly in regards to the organization of the functional map of visual space.

For analysis projection patterns of Isl2-GFP RGCs in relation to all RGCs adult mice were anesthetized as above. Intraocular injections of fluorescently-tagged cholera toxin subunit B (CTB-555, 2 mg/mL in PBS) were made with a pulled glass needle, as described previously (Pfeiffenberger et al., 2005). One day after intraocular injection animals were sacrificed and intracardially perfused with PBS and 4% PFA. Brains were dissected out and fixed overnight. To enhance the GFP signal, the cortex and dura overlying the SC was removed and brains were incubated in blocking solution (in PBS: 10% goat serum, 0.25% Triton X-100, 0.01% sodium azide) for 4 hours at room temperature. Primary antibody against GFP was added to the blocking solution (1:1000, Invitrogen) and brains were incubated for 48 hours on a shaking platform at 4 °C. Brains were washed in PBS 5X for 1 hour each and incubated in Alexafluor-488-conjugated secondary antibody (1:1000, Invitrogen) overnight on a shaking platform at 4 °C. The following day, brains were washed in PBS 5X for 1 hour each before imaging.

Quantitative analysis of anatomical images

The fluorescent intensity of signal for both bulk-labeled RGCs and Isl2-GFP were plotted as a function of position along the A–P axis at three parasagittal planes along the M–L axis. For each SC, the average correlation coefficient at the corresponding parasagittal planes and fluorescent signal of all other SCs was calculated. For each fluorescent signal (All RGCs vs. Isl2-GFP RGCs), the correlation index was calculated by determining the mean average correlation coefficient at each of three parasagittal planes. A one-tailed, unpaired student's t-test was used for statistical analysis of significance. Data are presented as mean +/− S.E.M.

Modeling of retinotopic map formation

We followed previous modeling studies of to simulate map formation in the SC (Tsigankov and Koulakov, 2010; 2006). Briefly, the SC is represented as an N by N matrix (N=100) of termination sites for RGC axons. The initial map is random. On each step of the optimization procedure, two RGC axons in SC are chosen randomly and exchanged with the probability $p = 1/[1 + \exp(\Delta E)]$, where ΔE is the change in adhesive energy due to the exchange. The formation of retinotopic map in SC depends on two components, graded chemical guidance cues (ΔE_{chem}) and activity dependent refinement (ΔE_{act}), in the following form: $\Delta E = \Delta E_{chem} + \Delta E_{act}$.

The contribution of chemical guidance cues is modeled by the following formula: $E_{chem} = \Sigma_i \alpha * R_A(i) * L_A(r_i) - \beta * R_B(i) * L_B(r_i)$, where $R_A(i)$ represents the EphA receptor level of point (i) in retina and $L_A(r_i)$ represents ephrin-A ligand level in its target point in SC; $R_B(i)$ and $L_B(r_i)$ simulate levels of receptors and ligands that have graded expressions and are required for map formation along dorsoventral axis; and $\alpha=\beta=120$ describe the strength of contributions.

The expression levels of these components are simulated following the original model found in (Tsigankov and Koulakov, 2006): $R_A(x) = \exp(-x/N) - \exp(x/N - 2)$ and $L_A(x) = \exp(x/N - 1) - \exp(-1 - x/N)$, where $x = 1 \ldots N$ is the coordinate along the N-T axis.

$R_B(y) = \exp(-y/N)$; $L_B(y) = \exp(-y/N)$, where y is the D-V coordinate.

To model the contribution of the extra EphA3 expressed in the retinas of *Isl2-EphA3* knock-in mice, a factor ΔR was added to R_A to every other cell in the retinal matrix. Following (Tsigankov and Koulakov, 2010), the value of ΔR was set to 0.70 to model the homozygous *Isl2-EphA3* knock-in and to 0.35 to model the heterozygote.

The contribution of activity-dependent process is modeled as: $E_{act} = -\gamma/2\Sigma_{i\,j}C_{ij}U(r_i - r_j)$, where $\gamma = 0.30$ is the strength parameter; $C_{i\,j}$ is the cross-correlation of neuronal activity between two RGCs during retinal waves; and U simulates the overlap between two SC cells. Here, we use $C_{i\,j} = \exp(-r/R)$, where r is retinal distance between axons i and j and R = 0.11*N and $U(r) = \exp(-r^2/(2d^2))$, where r is the distance between two SC points and d = 5 is the range of Hebbian attraction in the SC.

Supplementary Material

Refer to Web version on PubMed Central for supplementary material.

ACKNOWLEDGEMENTS

This work was supported by NIH grants (R01-EY02874 to M.P.S. and R01-EY014689 to D.A.F.) a Whitehall Foundation Grant (2013-08-41 to J.W.T.) and a Brain and Behavior Foundation NARSAD Young Investigator Grant (21259 to J.W.T.). M.T.O. was supported by an NIH Training Program for the Visual Sciences (T32-EY007120).

REFERENCES

Ackman JB, Burbridge TJ, Crair MC. Retinal waves coordinate patterned activity throughout the developing visual system. Nature. 2012; 490:219–225. [PubMed: 23060192]

Bevins N, Lemke G, Reber M. Genetic dissection of EphA receptor signaling dynamics during retinotopic mapping. J Neurosci. 2011; 31:10302–10310. [PubMed: 21753007]

Brown A, Yates PA, Burrola P, Ortuño D, Vaidya A, Jessell TM, Pfaff SL, O'Leary DD, Lemke G. Topographic mapping from the retina to the midbrain is controlled by relative but not absolute levels of EphA receptor signaling. Cell. 2000; 102:77–88. [PubMed: 10929715]

Cang J, Niell C, Liu X, Pfeiffenberger C, Feldheim D, Stryker M. Selective disruption of one cartesian axis of cortical maps and receptive fields by deficiency in ephrin-As and structured activity. Neuron. 2008a; 57:511–523. [PubMed: 18304481]

Cang J, Feldheim DA. Developmental mechanisms of topographic map formation and alignment. Annu Rev Neurosci. 2013; 36:51–77. [PubMed: 23642132]

Cang J, Kaneko M, Yamada J, Woods G, Stryker MP, Feldheim DA. Ephrin-As guide the formation of functional maps in the visual cortex. Neuron. 2005a; 48:577–589. [PubMed: 16301175]

Cang J, Rentería RC, Kaneko M, Liu X, Copenhagen DR, Stryker MP. Development of precise maps in visual cortex requires patterned spontaneous activity in the retina. Neuron. 2005b; 48:797–809. [PubMed: 16337917]

Cang J, Wang L, Stryker MP, Feldheim DA. Roles of ephrin-As and structured activity in the development of functional maps in the superior colliculus. J Neurosci. 2008b; 28:11015–11023. [PubMed: 18945909]

Chandrasekaran AR, Plas DT, Gonzalez E, Crair MC. Evidence for an instructive role of retinal activity in retinotopic map refinement in the superior colliculus of the mouse. J Neurosci. 2005; 25:6929–6938. [PubMed: 16033903]

Feinberg EH, Meister M. Orientation columns in the mouse superior colliculus. Nature. 2015; 519:229–32. [PubMed: 25517100]

Feldheim DA, Kim YI, Bergemann AD, Frisén J, Barbacid M, Flanagan JG. Genetic analysis of ephrin-A2 and ephrin-A5 shows their requirement in multiple aspects of retinocollicular mapping. Neuron. 2000; 25:563–574. [PubMed: 10774725]

Frisén J, Yates PA, McLaughlin T, Friedman GC, O'Leary DD, Barbacid M. Ephrin-A5 (AL-1/RAGS) is essential for proper retinal axon guidance and topographic mapping in the mammalian visual system. Neuron. 1998; 20:235–243. [PubMed: 9491985]

Gaze, RM. Company of Biologists. Growth and the development of pattern. Cambridge; New York: Cambridge University Press; 1981.

Golding B, Pouchelon G, Bellone C, Murthy S, Di Nardo AA, Govindan S, Ogawa M, Shimogori T, Lüscher C, Dayer A, et al. Retinal input directs the recruitment of inhibitory interneurons into thalamic visual circuits. Neuron. 2014; 81:1057–1069. [PubMed: 24607228]

Grimbert F, Cang J. New model of retinocollicular mapping predicts the mechanisms of axonal competition and explains the role of reverse molecular signaling during development. J Neurosci. 2012; 32:9755–9768. [PubMed: 22787061]

Grubb MS, Rossi FM, Changeux J-P, Thompson ID. Abnormal functional organization in the dorsal lateral geniculate nucleus of mice lacking the beta 2 subunit of the nicotinic acetylcholine receptor. Neuron. 2003; 40:1161–1172. [PubMed: 14687550]

Hickey TL, Guillery RW. Variability of laminar patterns in the human lateral geniculate nucleus. J Comp Neurol. 1979; 183:221–246. [PubMed: 762256]

Huberman AD, Stellwagen D, Chapman B. Decoupling eye-specific segregation from lamination in the lateral geniculate nucleus. J Neurosci. 2002; 22:9419–9429. [PubMed: 12417667]

Kaas JH, Guillery RW. The transfer of abnormal visual field representations from the dorsal lateral geniculate nucleus to the visual cortex in Siamese cats. Brain Res. 1973; 59:61–95. [PubMed: 4747773]

Kaas JH, Huerta MF, Weber JT, Harting JK. Patterns of retinal terminations and laminar organization of the lateral geniculate nucleus of primates. J Comp Neurol. 1978; 182:517–553. [PubMed: 102662]

Kalatsky VA, Stryker MP. New paradigm for optical imaging: temporally encoded maps of intrinsic signal. Neuron. 2003; 38:529–545. [PubMed: 12765606]

Koulakov AA, Tsigankov DN. A stochastic model for retinocollicular map development. BMC Neurosci. 2004; 5:30–30. [PubMed: 15339341]

Lee D, Malpeli JG. Global form and singularity: modeling the blind spot's role in lateral geniculate morphogenesis. Science. 1994; 263:1292–1294. [PubMed: 8122115]

Lim Y-S, Mclaughlin T, Sung T-C, Santiago A, Lee K-F, O'Leary DDM. p75(NTR) mediates ephrin-A reverse signaling required for axon repulsion and mapping. Neuron. 2008; 59:746–758. [PubMed: 18786358]

Mclaughlin T, Torborg CL, Feller MB, O'Leary DDM. Retinotopic map refinement requires spontaneous retinal waves during a brief critical period of development. Neuron. 2003; 40:1147–1160. [PubMed: 14687549]

Meister M, Wong RO, Baylor DA, Shatz CJ. Synchronous bursts of action potentials in ganglion cells of the developing mammalian retina. Science. 1991; 252:939–943. [PubMed: 2035024]

Nicol X, Voyatzis S, Muzerelle A, Narboux-Nême N, Südhof TC, Miles R, Gaspar P. cAMP oscillations and retinal activity are permissive for ephrin signaling during the establishment of the retinotopic map. Nat Neurosci. 2007; 10:340–347. [PubMed: 17259982]

Pfeiffenberger C, Cutforth T, Woods G, Yamada J, Rentería RC, Copenhagen DR, Flanagan JG, Feldheim DA. Ephrin-As and neural activity are required for eye-specific patterning during retinogeniculate mapping. Nat Neurosci. 2005; 8:1022–1027. [PubMed: 16025107]

Pfeiffenberger C, Yamada J, Feldheim DA. Ephrin-As and patterned retinal activity act together in the development of topographic maps in the primary visual system. J Neurosci. 2006; 26:12873–12884. [PubMed: 17167078]

Rashid T, Upton AL, Blentic A, Ciossek T, Knöll B, Thompson ID, Drescher U. Opposing gradients of ephrin-As and EphA7 in the superior colliculus are essential for topographic mapping in the mammalian visual system. Neuron. 2005; 47:57–69. [PubMed: 15996548]

Reber M, Burrola P, Lemke G. A relative signalling model for the formation of a topographic neural map. Nature. 2004; 431:847–853. [PubMed: 15483613]

Simon DK, O'Leary DD. Development of topographic order in the mammalian retinocollicular projection. J Neurosci. 1992; 12:1212–1232. [PubMed: 1313491]

Stafford BK, Sher A, Litke AM, Feldheim DA. Spatial-temporal patterns of retinal waves underlying activity-dependent refinement of retinofugal projections. Neuron. 2009; 64:200–212. [PubMed: 19874788]

Stryker MP. Precise development from imprecise rules. Science. 1994; 263:1244–1245. [PubMed: 8122106]

Suetterlin P, Drescher U. Target-independent EphrinA/EphA-mediated axon-axon repulsion as a novel element in retinocollicular mapping. Neuron. 2014; 84:740–752. [PubMed: 25451192]

Triplett JW. Molecular guidance of retinotopic map development in the midbrain. Curr Opin Neurobiol. 2014; 24:7–12. [PubMed: 24492072]

Triplett JW, Owens MT, Yamada J, Lemke G, Cang J, Stryker MP, Feldheim DA. Retinal input instructs alignment of visual topographic maps. Cell. 2009; 139:175–185. [PubMed: 19804762]

Triplett JW, Pfeiffenberger C, Yamada J, Stafford BK, Sweeney NT, Litke AM, Sher A, Koulakov AA, Feldheim DA. Competition is a driving force in topographic mapping. Proceedings of the National Academy of Sciences. 2011; 108:19060–19065.

Triplett JW, Wei W, Gonzalez C, Sweeney NT, Huberman AD, Feller MB, Feldheim DA. Dendritic and axonal targeting patterns of a genetically-specified class of retinal ganglion cells that participate in image-forming circuits. Neural Dev. 2014; 9:1–13. [PubMed: 24405572]

Tsigankov DN, Koulakov AA. A unifying model for activity-dependent and activity-independent mechanisms predicts complete structure of topographic maps in ephrin-A deficient mice. J Comput Neurosci. 2006; 21:101–114. [PubMed: 16823525]

Tsigankov D, Koulakov AA. Sperry versus Hebb: Topographic mapping in Isl2/EphA3 mutant mice. BMC Neurosci. 2010; 11:155. [PubMed: 21190559]

Xu W, Orr-Urtreger A, Nigro F, Gelber S, Sutcliffe CB, Armstrong D, Patrick JW, Role LW, Beaudet AL, De Biasi M. Multiorgan autonomic dysfunction in mice lacking the beta2 and the beta4 subunits of neuronal nicotinic acetylcholine receptors. Journal of Neuroscience. 1999; 19:9298–9305. [PubMed: 10531434]

Yates PA, Roskies AL, McLaughlin T, O'Leary DD. Topographic-specific axon branching controlled by ephrin-As is the critical event in retinotectal map development. J Neurosci. 2001; 21:8548–8563. [PubMed: 11606643]

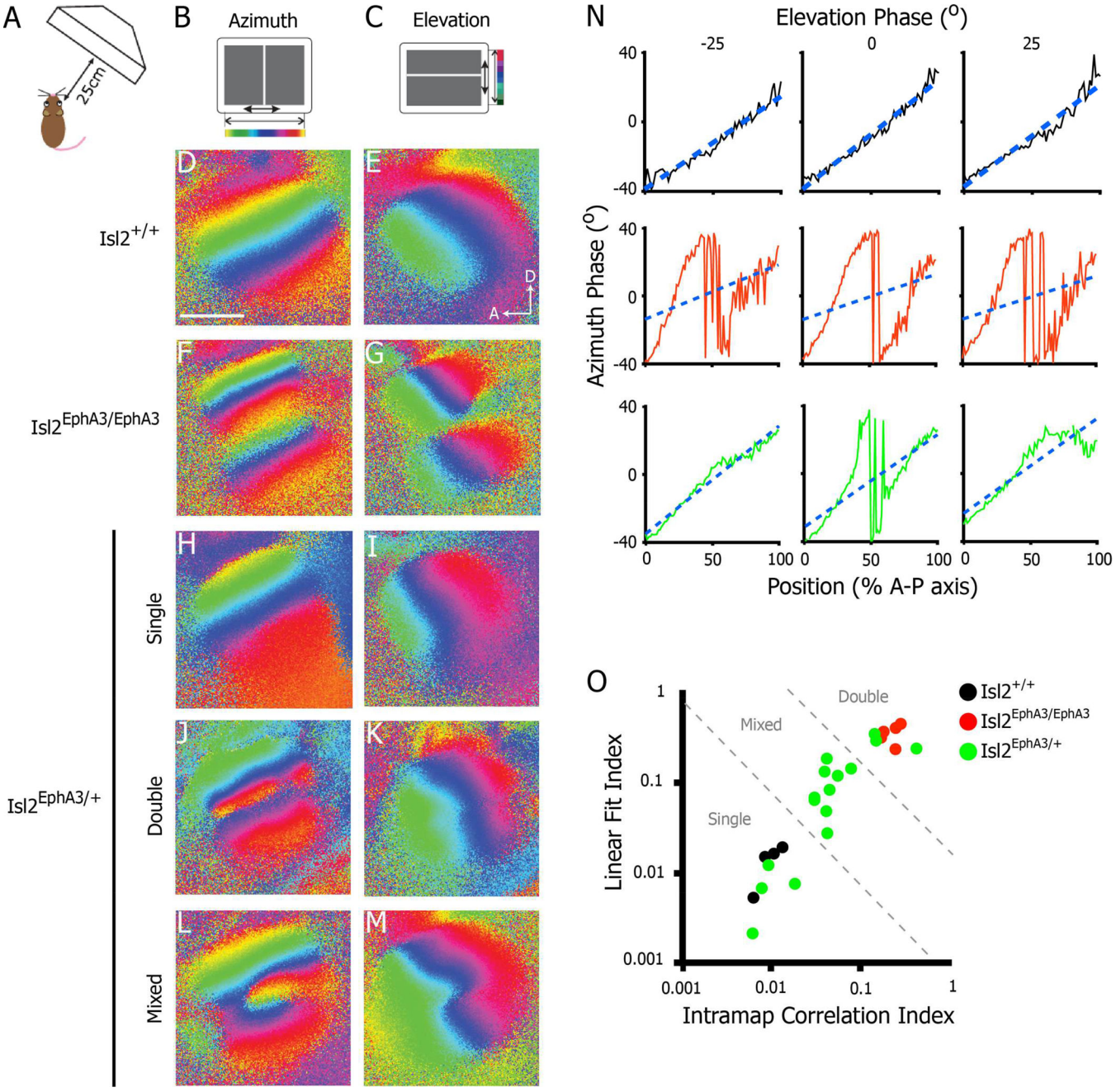

Figure 1.

Heterogeneity in the functional azimuth representation in the SC of Isl2$^{EphA3/+}$ mice. A–C) Schematics of intrinsic signal optical imaging paradigm. Drifting vertical (azimuth, B) and horizontal (elevation, C) are presented on a screen placed 25 cm from an anesthetized mouse. Regions of the SC responding to different regions of the visual field are pseudo-colored as indicated. D-E) Azimuth (D) and elevation (E) representations in a wild type SC reveal a single coherent map in each case (n = 4). F–G) Imaging of SC responses in an Isl2$^{EphA3/EphA3}$ mouse reveal a complete duplication of azimuth (F) and a discontinuity at the border of these maps in the elevation representation (G) (n = 5). H-M) Imaging of SC

responses in an Isl2$^{EphA3/+}$ reveals a variety of organizations in the azimuth representations: single (H), double (J) and mixed-type (L) (n = 16). N) Phase plots of the azimuth representation along the anterior-posterior axis of the SC at three isoelevation points from Isl2$^{EphA3/+}$ mice exhibiting a single map organization (top row), double organization (middle row) and mixed organization (bottom row). Blue dashed lines represent the best linear fit for each phase plot. O) Map organizations plotted by two quantitative indices. Isl2$^{+/+}$ maps (black dots) fall within the region determined to be single, Isl2$^{EphA3/EphA3}$ maps (red dots) fall within the double zone, and Isl2$^{EphA3/+}$ maps (green dots) are distributed across single, double and mixed regions of the plot. *bar, 0.5 mm; A, anterior; D, dorsal*

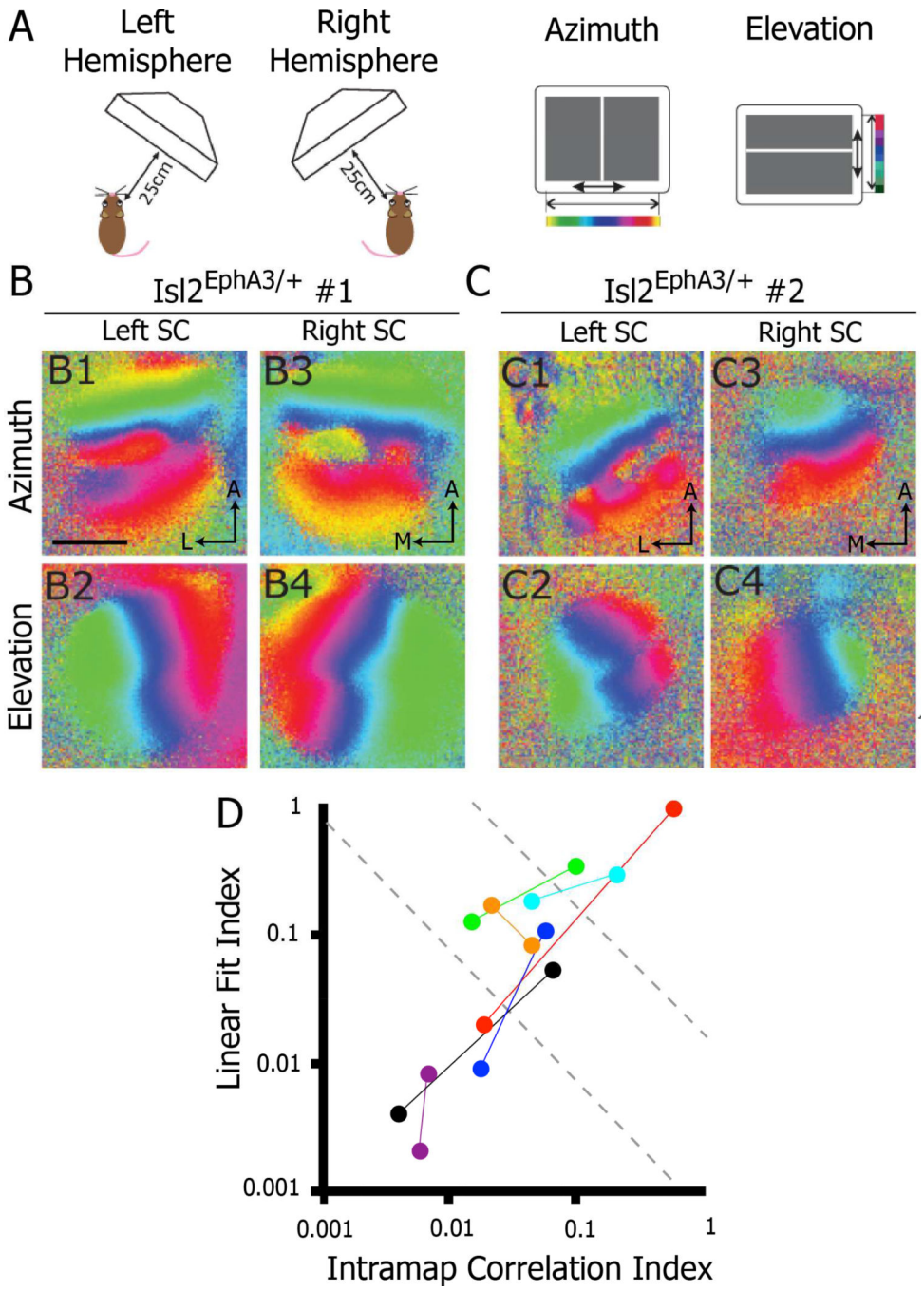

Figure 2.

Bilateral heterogeneity of azimuth representation in opposing collicular hemispheres of Isl2$^{EphA3/+}$ mice. A) Schematics of imaging paradigm to evaluate azimuth and elevation representations in each SC hemisphere of a single mouse. B & C) Azimuth and elevation representations in the left and right SC of two different Isl2$^{EphA3/+}$ mice reveals heterogeneity between hemispheres (n = 7). D) Map organizations of Isl2$^{EphA3/+}$ mice in which both SCs were imaged plotted by two quantitative indices. Each pair of colored dots

represents the two SCs of an individual Isl2$^{EphA3/+}$ mouse. *bar, 0.5 mm; A, anterior; L, lateral; M, medial*

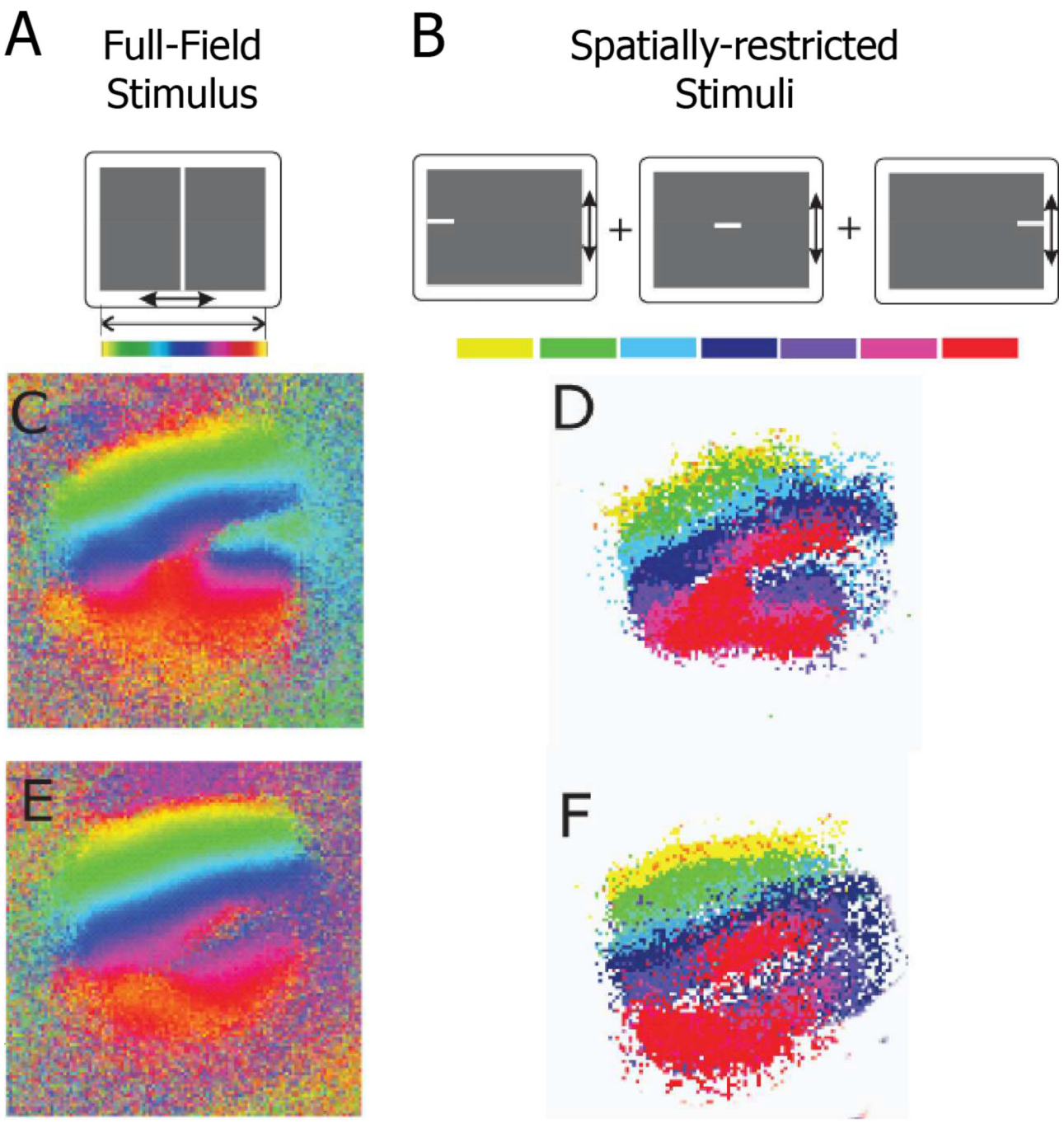

Figure 3.

Lack of functional suppression in the SC of Isl2$^{EphA3/+}$ mice. A & B) Schematics of full-field (A) and spatially-restricted (B) stimuli used to determine if subsets of SC regions may be functionally suppressed. C-F) Azimuth representations from the SC of two Isl2$^{EphA3/+}$ mice derived from the use of full-field stimulus (C & E) or spatially-restricted stimuli (D & F).

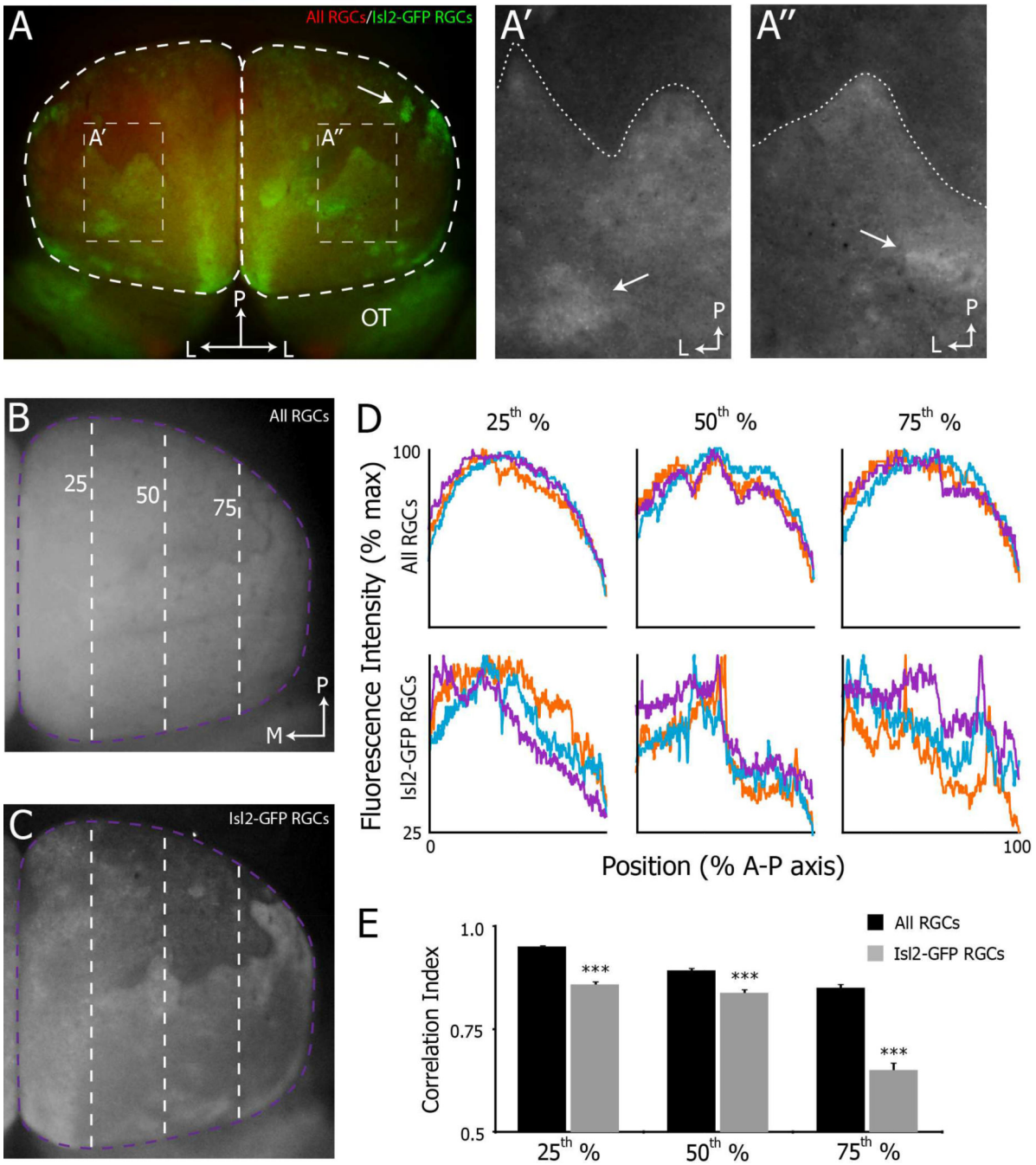

Figure 4.

Heterogeneity in the projection patterns of Isl2^{+} RGCs in Isl2$^{EphA3/+}$ mice. A) Dorsal views of Isl2-GFP projections to the SC (white dashed regions) in whole mount of an adult Isl2$^{EphA3/+}$ mice reveal distinct organizations. A'-A") Enlarged views of regions of interest indicated in (A). Dashed lines indicate the "border" between regions of high and low Isl2-GFP^{+} RGC innervation. Arrows indicate clusters of Isl2-GFP^{+} RGC terminals. B & C) Dorsal views of the projections of all RGCs (B) and Isl2-GFP^{+} RGCs (C) to the left SC of an adult Isl2$^{EphA3/+}$ mouse. Dashed purple and green lines are located at the 25th, 50th and

75^{th} percentile of the medial-lateral axis of the SC. D) Plots of the fluorescence intensity signal of all RGCs (top row) and Isl2-GFP^{+} RGCs (bottom row) from three representative $Isl2^{EphA3/+}$ SCs. Intensity was plotted as a function of position along the A-P axis at three different parasagittal planes of the M-L axis, indicated by dashed lines in (B & C). E) Quantification of the average correlation indices at each parasagittal plane for all RGCs (black bars, n = 8) and Isl2-GFP RGCs (grey bars, n = 11). *bar, 0.5 mm; L, lateral; P, posterior; OT, optic tract; M, medial; A, anterior; **, $p < 0.01$ vs. All RGCs; ***, $p < 0.001$ vs. All RGCs*

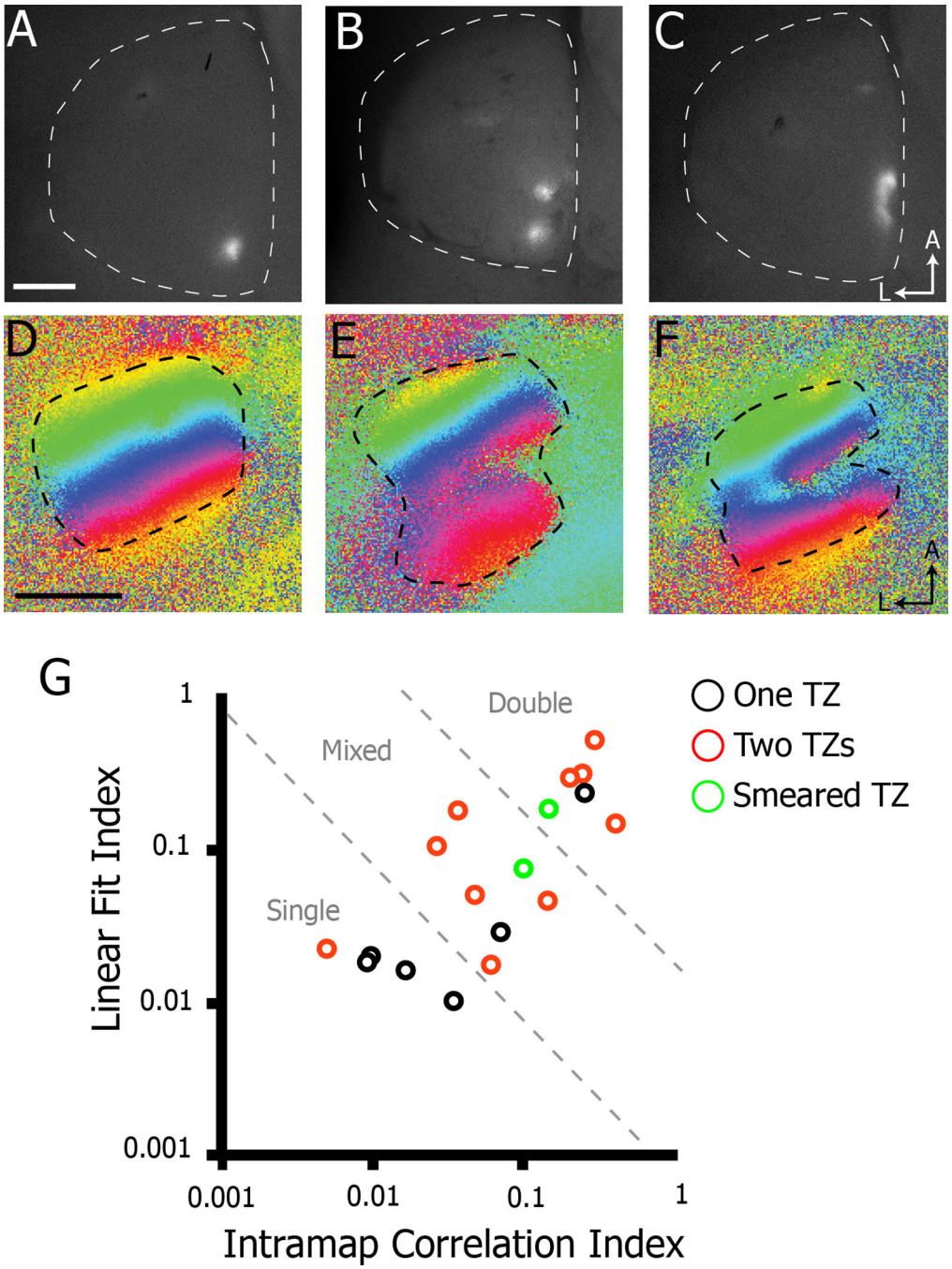

Figure 5.

Correlation of anatomical and functional map organizations in Isl2$^{EphA3/+}$ mice. A–C) Dorsal views of the SCs of Isl2$^{EphA3/+}$ mice in which the nasal retina was focally labeled with DiI reveals one (A), two (B), or a smeared (C) termination zone (TZ) (n = 18). D–E) Corresponding functional representations of azimuth to the Isl2$^{EphA3/+}$ mice labeled in A–C. G) Map organizations of traced and imaged Isl2$^{EphA3/+}$ SCs plotted by two quantitative indices. Axon labeling resulting in one (black circles), two (red circles) or smeared (green circles) TZs is indicated. *bar, 0.5 mm; A, anterior; L, lateral*

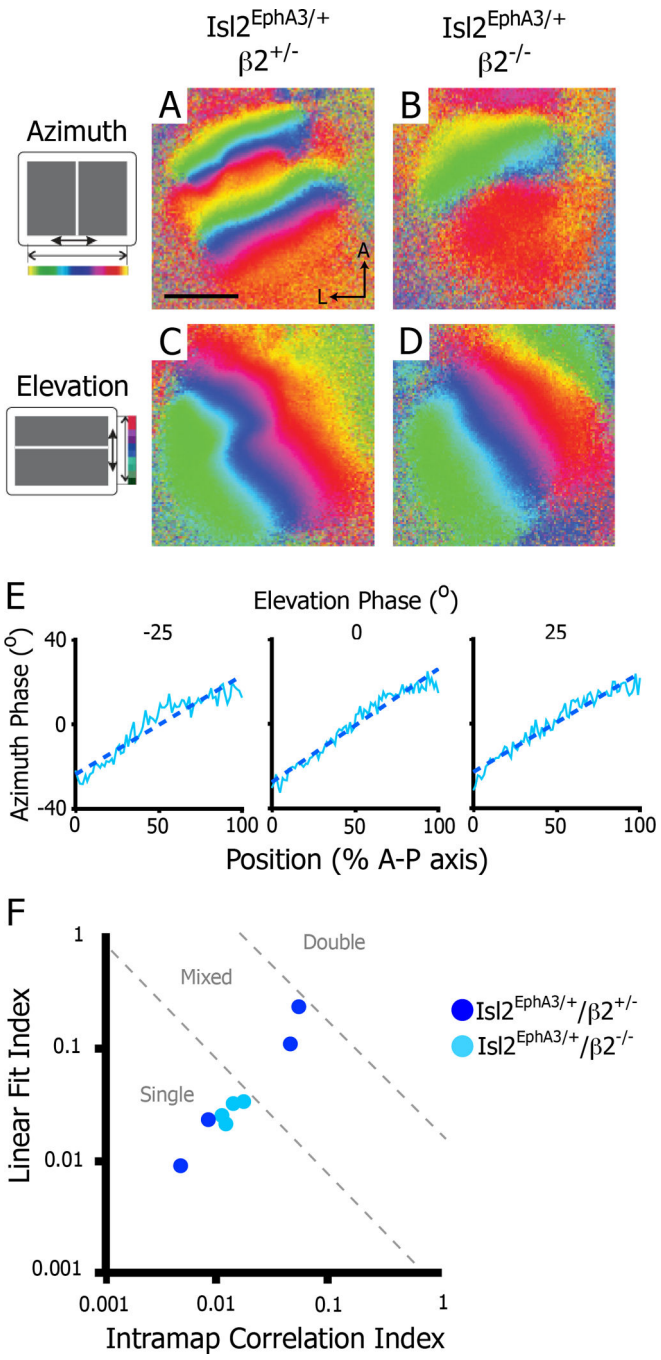

Figure 6.

Disruption of retinal waves eliminates heterogeneity in the azimuth representation in the SC of Isl2$^{EphA3/+}$ mice. A–B) Intrinsic signal optical imaging of the azimuth representation in Isl2$^{EphA3/+}$/β2$^{+/-}$ (n = 4) (A) and Isl2$^{EphA3/+}$/β2$^{-/-}$ (n = 4) (B). C–D) Intrinsic signal optical imaging of the elevation representation in Isl2$^{EphA3/+}$/β2$^{+/-}$ (C) and Isl2$^{EphA3/+}$/β2$^{-/-}$ (D). E) Phase plots of the azimuth representation along the anterior-posterior axis of the SC at three isoelevation points from an Isl2$^{EphA3/+}$/b2$^{-/-}$ SC. F) Map organizations of Isl2$^{EphA3/+}$/b2$^{+/-}$

(dark blue dots) and Isl2$^{EphA3/+}$/b2$^{-/-}$ (light blue dots) SCs plotted by two quantitative indices. *bar, 0.5 mm; A, anterior; L, lateral*

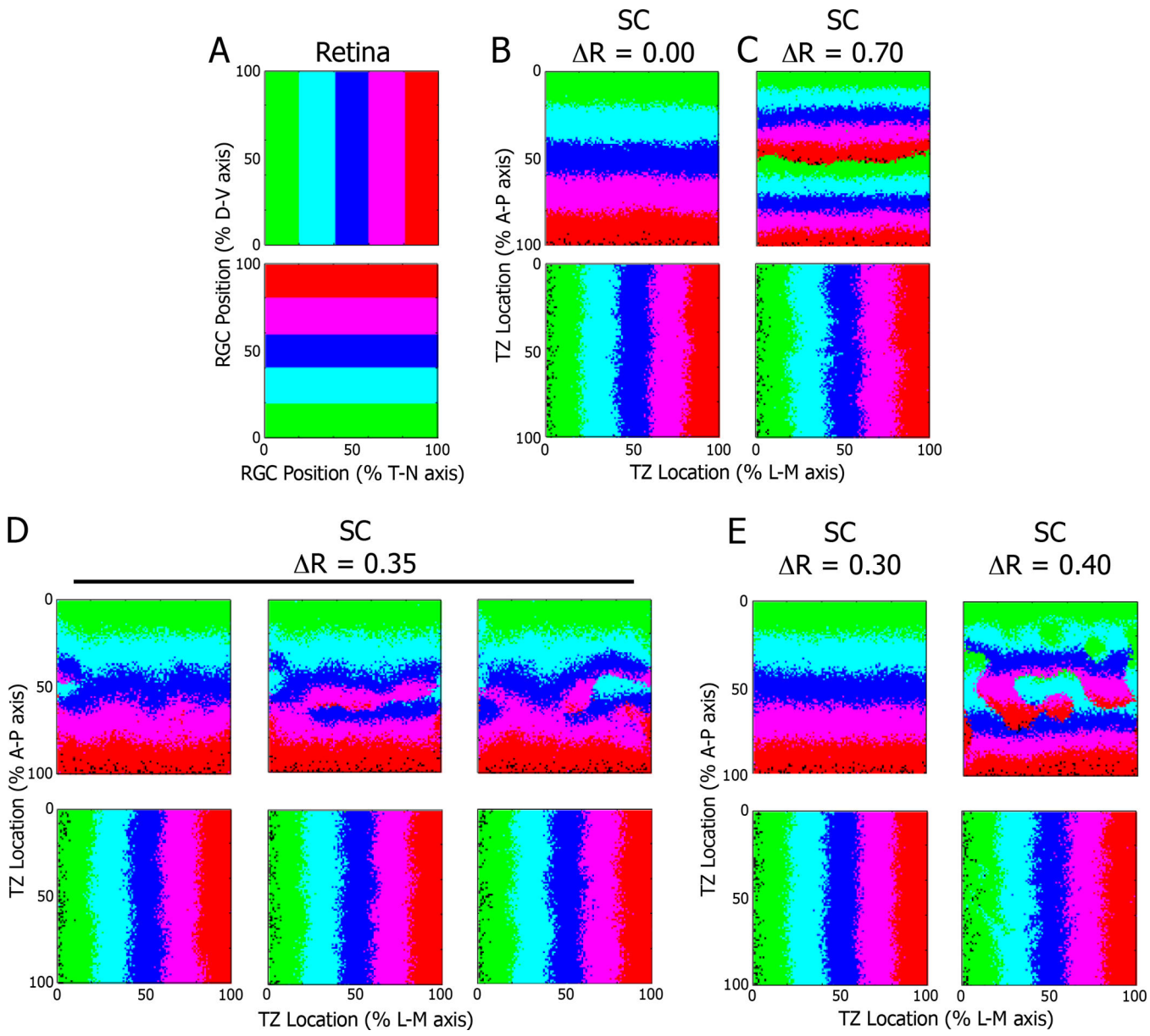

Figure 7.

Replication of heterogeneity in a mathematical model of retinocollicular mapping. A) Representations of the retina as a 100 × 100 matrix, with corresponding color-coding based on position along the D–V and T–N axes. B) Results of simulations of the model run with the value for exogenous EphA3 expression (ΔR) set to 0.00 (for wild type) or 0.70 (for $Isl2^{EphA3/EphA3}$) reveal predicted organizations of projections along the A-P and L-M axes of the SC. D) Representative examples of three distinct simulations of the model when ΔR was set to 0.35 (for $Isl2^{EphA3/+}$ mice), reveals a heterogeneity in the organization of inputs along the A-P axis. Minor changes in ΔR around 0.35 yielded consistent map organizations that were singular (0.30) or doubled (0.40). *D, dorsal; V, ventral; T, temporal; N, nasal; A, anterior; P, posterior; L, lateral; M, medial*